

Ensemble CNN and Uncertainty Modeling to Improve Automatic Identification/Segmentation of Multiple Sclerosis Lesions in Magnetic Resonance Imaging

Giuseppe Placidi¹ Luigi Cinque² Daniela Iacoviello³ Filippo Mignosi⁴
Matteo Polsinelli¹

¹ A2VI-lab, c/o Department of MeSVA, University of LAquila, Via Vetoio Coppito 2,
67100 - LAquila, ITALY

giuseppe.placidi@univaq.it

² Department of Computer Science, Sapienza University of Rome, Via Salaria 113,
00198 - Roma, ITALY

³ Department of Computer, Control and Management Engineering Sapienza University
of Rome, Rome, Italy

⁴ Department of DISIM, University of LAquila, Via Vetoio Coppito, 67100 - LAquila,
ITALY

Abstract

To date, several automated strategies for identification/segmentation of Multiple Sclerosis (MS) lesions with the use of Magnetic Resonance Imaging (MRI) have been presented, but they are outperformed by human experts, from whom they act very differently. This is mainly due to: the ambiguity originated by MRI instabilities; peculiar variability of MS; non specificity of MRI regarding MS. Physicians partially manage the uncertainty generated by ambiguity relying on radiological/clinical/anatomical background and experience. To emulate human diagnosis, we present an automated framework for identification/segmentation of MS lesions from MRI based on three pivotal concepts: 1. the modelling of uncertainty; 2. the proposal of two, separately trained, CNN, one optimized for lesions and the other for lesions with respect to the environment surrounding them, respectively repeated for axial, coronal and sagittal directions; 3. the definition of an ensemble classifier to merge the information collected by different CNN.

The proposed framework is trained, validated and tested on the 2016 MSSEG benchmark public data set from a single imaging modality, the FLuid-Attenuated Inversion Recovery (FLAIR). The comparison with the ground-truth and with each of 7 human raters, proves that there is no significant difference between the automated and the human raters.

1 Introduction

Multiple Sclerosis (MS) is a degenerative disease mainly affecting white matter (WM) and spinal cord, with a very heterogeneous clinical presentation across patients both in severity and symptoms [46].

The origins of the disease are not well understood but characteristic signs of tissue degeneration are recognizable by the presence of lesions and brain atrophy. Most of MS signs can be observed through Magnetic Resonance Imaging (MRI) which has become the elective mini-invasive tool for MS [16]. Focal lesions are primarily visible in the white matter on structural MRI, observable as hyper-intensities on T₂-weighted images (T₂w), on proton-density images (PD), or on FLuid-Attenuated Inversion Recovery images (FLAIR), and as hypo-intensities on T₁-weighted images (T₁w).

Physicians often use FLAIR images for WM lesion detection and other modalities mostly to ascertain the presence of cortical lesions.

An examination consists in thousands of images mostly collected pre and post contrast administration. MRI is used routinely in clinical practice but it is unspecific for MS and not well correlated to the impairment progression, to the neuro-plasticity and to the effects of demyelination of nerves, the last being a critical effect which is invisible to MRI. In a MS patient, the "healthy" brain tissue is usually referred as "apparently healthy" [16]. In addition, often lesions and healthy tissue are present in the same

place, thus resulting in the partial volume effect (PVE). Regarding MRI, healthy anatomical structures similar to lesions and close to lesions could contribute to create further ambiguity. Moreover, there is a huge variability in images due to differences in scanners, magnetic field strength/homogeneity and tuning of parameters [37]. Efforts have been made to standardize MRI amplitude [10] but results are still unsatisfactory due to the huge set of parameters to be tuned. The consequence of the above phenomenons are ambiguities and disagreement among radiologists (inter-raters variability) as well as uncertainty in a same radiologist (intra-rater variability) mainly in defining the borders of the lesions, but also in labeling whole regions. This could make the manual segmentation, besides long and boring, also inaccurate, especially when quantitative evaluations are required, despite the ability of radiologists in relying on unexpressed anatomical/clinical background, on knowledge about MS and its symptoms.

Several automatic frameworks have been recently proposed and reviewed [3, 11, 13, 19, 20, 38, 60]. Despite the huge efforts, to date the results are still far from those of human experts. Actually, this has led to an increase in the model complexity not corresponding to the expected improvement [34]. Automated strategies are not robust to MRI variability, not even sufficiently able to model medical knowledge, human operational capacity and flexibility. Furthermore, the reasoning methodology used by radiologists for volume analysis, consisting in 2D axial slices with a continuous view of coronal and sagittal slices for confirmation [16, 49], is not fully imitated by automatic strategies. A recent paper [33] highlights the importance of using 3D CNN in MS lesion segmentation, though other recent frameworks [48, 56] prefer ensembles of 2D U-net models, in a way which is similar to the human methodology. Human methodology is empowered by the fact that spatial resolution is often not the same along the three axes with a prevalence for axial planes. However, the uncertainty affecting radiologists during classification is not reported in the public data sets: a binary choice is often insufficient to represent the evaluation of an expert. If represented, the uncertainty could greatly help an automatic strategy to better segment also undoubted lesions. This pushed to investigate on uncertainty in medical data [4] and on the effect that the rater style could transfer in terms of uncertainty to an automated strategy [53].

Implicit information in automated methods is difficult to be modelled and more, if introduced with external supports (dictionary, anatomical atlases, etc.) [31], is often insufficient to fill the gap with human experts.

We aim at filling this gap, both in performance and in reasoning, by proposing a framework which includes: 1) the classification of uncertainty as an intermediate class between the background and lesions; 2) the optimization of two CNN (2D U-net models), one for the class lesion and one for the class background to contextualize lesions with respect to the surrounding anatomical structures for the three spatial directions (axial, coronal and sagittal); 3) the definition of an ensemble classifier to merge the information collected by all CNN.

To obtain our goal we: use the publicly available large-scale benchmark MRI database and corresponding ground truth proposed in 2016 MICCAI MS Lesion Segmentation Challenges, MSSEG [1]; define the uncertain regions with the help of the binary classifications of 7 human raters in MSSEG; apply the framework just on FLAIR images.

These choices allow to: compare the proposed framework with competitive automated strategies and human experts; demonstrate that the uncertain reasoning modelling could help in reducing the ambiguity and complexity of the, intrinsically uncertain, problem; demonstrate that a single imaging sequence, FLAIR, is sufficient for MS lesion identification/segmentation in WM. It is implicit that the framework applies to WM lesions and not on cortical lesions, being these last absent in MSSEG.

The manuscript is structured as follows: Section 2 presents a review of automatic approaches to MS lesion identification/segmentation, in particular those using CNN; Section 3 describes the proposed framework in the context of the used data set, the defined three-class consensus used for training, the proposed CNN architecture and the ensemble system; Section 4 details the metrics used for comparison; Section 5 reports and discusses experimental results; Section 6 concludes the paper and presents some constructive hints for future improvements.

2 Related work

Medical image analysis is greatly performed with automated methods, mostly involving deep learning [29, 30, 32, 36, 55]. Automated MS lesion identification/segmentation is still an active field of research and several methods have been provided in the last decade and well reviewed along time [11, 13, 28, 60] with an emerging role of AI-based methods [2].

Automated strategies can be classified into three main groups: methods using pre-selected features

modelling (PSFM), methods using a-priori information modelling (APIM) and methods using deep learning modelling (DLM).

PSFM calculate pre-selected features and learn from previously segmented training images to separate lesions from healthy tissue [62]. Some PSFM use a large set of features and select the more discriminant ones through labelled training. Others use an atlas-based technique, employing topological and statistical atlases for WM lesion segmentation [43, 54]; another includes the usage of Decision Random Forests [18]. Similarly, a framework for segmentation of contrast-agent enhanced lesions using conditional random fields is defined in [26]. The work in [8] proposes a set of features, including contextual features, registered atlas probability maps and an outlier map, to automatically segment MS lesions through a voxel by voxel approach. A rotation-invariant multi-contrast non-local means segmentation is proposed in [21] for the identification and segmentation of lesions from 3D MRI images. Supervised learning by PSFM has been widely employed in tasks where the training database and the pre-selected feature set cover all possible cases [9]. Nevertheless, when the heterogeneity of the disease and the potential variability of imaging are large, as it occurs for MS and MRI, the dimension of the training database and, mostly, the choice of the pre-selected features are critical.

APIM does not require labelled training data to perform segmentation, but usually exploit some a-priori information, such as the intensity clustering[58], to model tissue distribution. In [6], a likelihood estimator to model the distribution of intensities in healthy brain MR images is presented. Other methods use threshold with post processing refinement [41] or are based on probabilistic models [47]. A big challenge for APIM is that the outliers are not specific for lesions because they could be due to artifacts, intensity inhomogeneity and small anatomical structures like blood vessels: this often produces false positives [7]. Moreover, APIM is strongly based on the information extracted and simplified by the knowledge of specific experts.

During the last years DLM has gained popularity in medical imaging especially with U-nets ad their variants [23, 35, 39, 63]. Though the dimension of the training database is also crucial in DLM, this has no concern regarding the pre-selection of features as in PSFM or regarding a-priori information modelling as in APIM. In particular CNN, compared to machine learning approaches, has achieved remarkable success in biomedical image analysis [7, 36, 55, 56]. DLM trains and learns to design features directly from data [5] and provides best results in MS lesion identification/segmentation, as recently confirmed in [3, 11, 13, 20, 25, 28, 52, 59, 60].

CNN applied to MS often use 2D spatial convolutional layers [5], others use 3D convolutional layers to incorporate 3D spatial information simultaneously [22, 40, 50, 51] or merge spatial with temporal information [38]. All these methods perform segmentation with a minimum lesion volume threshold to avoid the inclusion of small false positives.

Some methods improve the MS segmentation by retraining the CNN from the first layers, in a kind of self supervision [15], by hypothesizing that the those layers are more sensitive.

Among other recent works, hybrid models [14] allow to detect MS lesions by using textural features in combination with machine learning approaches, as Decision Tree (DT) and Support Vector Machines (SVM).

However, CNN performance is still far from that obtained by human experts or dramatically drops with other data sets [34].

3 The proposed framework

The framework we propose, sketched in Figure 1, consists of the following steps: 1) deep learning automatic classification, of the images (2D) composing the MRI model, in three classes: Background, Uncertainty and Lesion (capital letter to imply the concept 'class'), optimized for Lesion (lesions from inside) and for Lesion in the context of the surrounding environment, separately for axial, coronal and sagittal directions (resulting in 6 classifiers); 2) class fusion (separately for Lesion and Uncertainty, starting from Lesion) by performing the Union of the 2 axial segmentation (step 2a in Figure 1), followed by a majority vote taken from the remaining segmentations and used for confirmation of the class (if the class is not confirmed, this is downgraded (step 2b in Figure 1); 3) final output.

For the framework we propose, the following three hypotheses hold:

- 1) the MSSEG pre-processed data from just one single MRI modality, FLAIR, are the input of the framework;

- 2) the binary labelled ground-truth is revised to contain, besides Lesion and Background, also Uncertainty which is created from part of the original Background, leaving Lesion unchanged (see detailed description below);

3) the three considered classes are supposed to be ordered, Background < Uncertainty < Lesion: in our case, just Lesion and Uncertainty are the subjects of fusion and, for this reason, their downgrading consists in the passage from Lesion to Uncertainty and from Uncertainty to Background, respectively: the process starts from Lesion to allow Uncertainty fusion on the upgraded data set.

Step 2a of Figure 1 serves to include, besides common information, also complementary ones coming from the specificity of each of the two axial CNN and, at the same time, to model the reasoning of the radiologists that use axial orientation to make the first hypotheses. Step 2b is used to vote for each object resulting from the axial processing (Lesion or Uncertainty), its permanence in the assigned class, or its downgrading. Objects are confirmed when at least two of the other four raters (two coronal and two sagittal) agree with the axial classification. This ensures that false positives are greatly reduced, that 3D contextualization with the environment is maintained and that the model agrees with the radiologist’s reasoning.

The choices regarding the usage of one single imaging modality, the classification in three classes and the use of an ensemble framework are clarified below.

Being supervised, each classifier needs training, validation and test carried on by using data from a public data set. In what follows we first describe the used data set, the ternary ground truth, the CNN architecture, the used loss function, the hyper-parameters optimization and the ensemble, final, classification of Figure 1.

3.1 MSSEG data set

To allow a direct comparison and benchmark of the proposed framework with the state-of-the-art segmentation methodologies, we use the 2016 MSSEG data set [1]. In MSSEG, data were collected with several MRI scanners using different magnetic field strengths: 1.5T Siemens Aera, 3T Siemens Verio, 3T Philips Ingenia and 3T General Electric Discovery. The data set contains, for each examination, T_1 -w, T_1 -w gadolinium enhanced (T_1 -w Gd), T_2 -w, T_2 -FLAIR and PD -w images.

We have chosen MSSEG because it is a benchmark data set including 7 different classifications made by 7 different expert human raters and a consensus, the ground-truth, making it possible to compare our framework with human classifications, as well as with state of the art automatic strategies. For MSSEG, it has been asked the human raters to perform a binary segmentation (each voxel was identified as lesion/not lesion): the annotated data set has been composed by 15 training cases. Another subset of data, composed of 38 testing cases, has been left without annotation.

The images are anonymized and provided both in original form and pre-processed for user convenience.

Pre-processing refers to a series of mathematical adjustments to MR images before segmentation [45] for reducing the effects of noise and imaging artifacts, equalizing space, eliminating outliers and stabilizing the contrast.

Though the MSSEG data set contains images from 4 imaging modalities, in our framework we opt for the usage of one single modality (FLAIR) to: detect/segment MS lesions in WM; demonstrate that a single modality is sufficient for MS lesion identification/segmentation in WM; avoid that the potential gain of using multiple imaging modalities could be overcome by the drop in robustness and performance due to residual MRI instabilities after pre-processing.

Further, we divide the annotated MSSEG data set, composed by 15 subjects, in three subsets respectively for training, validation and test, as follows:

- the training data set contains examinations from 9 subjects, 3 subjects of each centre;
- the validation data set contains data from 3 subjects, one for each centre;
- the test data set contains the remaining data, from 3 subjects, one for each centre.

An exhaustive cross validation is performed while maintaining the proportions between centres. Once the data set is established, it is augmented by adding, for each image, 2 random rotations (between -13 and 13 degrees, 1 degree in resolution), 1 random scaling (between 1.1 and 1.3, 0.01 in resolution) and 1 gaussian random noise addition, 0 mean and 0.001A variance, where A is the maximum amplitude value in the examined volume.

The augmented data set, for each validation and orientation (axial, coronal and sagittal), contains 5216 images for training, 418 images for validation and 435 images for test.

The augmented data originated from the same dataset [1] used to train, validate and test the state of the art methods. In this way, we can indirectly compare our framework with the state of the art strategies by using, for them, the performance evaluation reported in the original manuscripts.

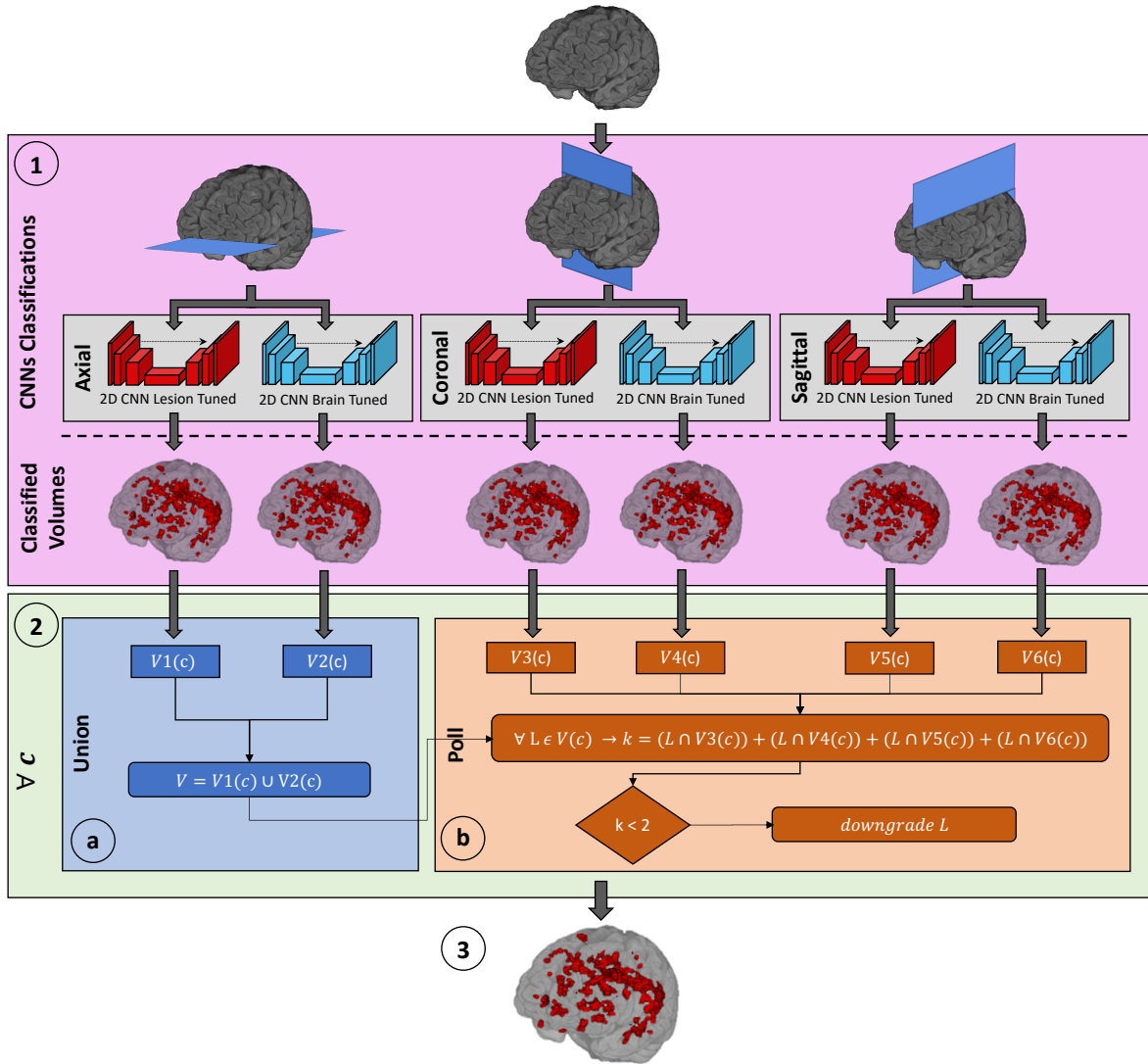


Figure 1: The proposed identification/segmentation pipeline which divides the brain tissue in three classes: healthy tissue (Background), tissue that has uncertain nature (Uncertainty), and MS lesions (Lesion). The strategy operates independently on axial, coronal and sagittal images, each processed by two separately trained U-nets, one optimized for Lesion, to directly focus on lesions, and the other optimized for contextualizing lesions with respect to the environment. It recombines the results by using the Union of axial volumes followed by a majority vote strategy on the coronal and sagittal volumes, for confirmation. Voxels whose classification is not confirmed are downgraded (Lesion becomes Uncertainty and Uncertainty becomes Background). The framework operates separately for Lesion and Uncertainty, starting from Lesion. In step 2b, the procedure is applied voxel by voxel: L is referred to each single voxel of the class $c \in \{Lesion, Uncertainty\}$.

3.2 Ternary ground-truth

In medical imaging it can be assumed that there is a single, unknown, true segmentation map of the underlying anatomy, and each human rater produces an approximation with variations reflecting individual experience.

In the opposite case, it can be assumed that the variable annotations from experts are all realistic and acceptable instances of the true segmentation.

As it often occurs, the truth is in the middle: some ambiguities are indeed due to human subjectivity or imperfections (extrinsic), while some others are due to the problem itself (intrinsic). In our problem, both are important, but intrinsic ambiguities have the highest role, being due both to MS presentation and to MRI non specificity: lesions are not well separated from healthy tissue in MS (due to PVE)

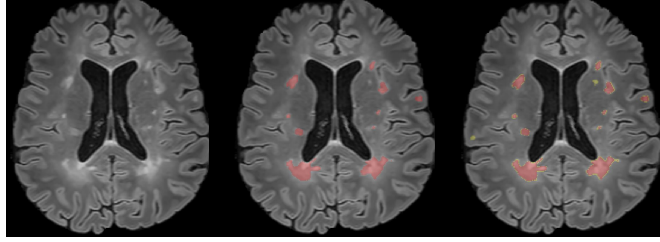


Figure 2: A sample FLAIR image from the MSSEG data set (left), the binary consensus (middle) and the proposed ternary consensus (right). The Lesion is annotated in red. In the ternary consensus, the Uncertainty is indicated in yellow.

and MRI is neither sufficiently specific for MS nor sufficiently precise. Regarding human subjectivity, it produces differences that are due to a mix of prior assumptions, like experience in the field, greater or lesser exploitation of additional meta-information (such as anatomical/radiological/clinical knowledge), mistakes or oversights which often are concentrated on small and/or low intensity lesions and lesion borders.

When raters are forced to provide a binary segmentation, as in MSSEG, they cannot express any doubt, whatsoever is the cause. The binary segmentation does not allow the representation of the intrinsic uncertainty and, furthermore, induces a human rater to assume polarized decisions which, from one side, could not correspond to what the rater really believes in and, from the other side, could be confusing and misleading for an automated strategy. In fact, ambiguous decisions might have been assumed by the rater in similar situations (an uncertain region could be considered healthy tissue in one case and lesion in another) which could influence the automated strategy [53].

If we want to train an automated method to recognize the problem-specific uncertainty, we have to integrate the binary ground-truth with human uncertainty (doubts). To maintain the original ground-truth, we just consider as Uncertainty the voxels that at least three of the seven human raters considered as lesions and the binary consensus had not. In this way, since we create space for the Uncertainty from the Background, the Lesion class of the binary consensus remains unchanged: this allows the comparison with state of the art strategies, performed on Lesion. The use of Uncertainty in this specific context is intended to reduce the uncertainty in identifying Lesion, hence to improve classification. A more accurate definition of the uncertainty, though interesting, is out the scope of the manuscript and deserves specific exploration.

The method we propose is quite different from other strategies used to define the uncertainty [20, 27], for the following motivations: 1) to maintain the original structure of Lesion; 2) to account for the uncertainty affecting both the problem and the raters; 3) to avoid the new class Uncertainty could prevent a direct comparison with other methods; 4) to quantify the performance gain the proposed framework could effectively get when the Uncertainty is introduced; 5) to allow the learning strategy to consider as uncertain not only lesion borders, as other Authors do [27], but also whole regions not necessarily connected to lesions. In fact, Uncertainty could regard both the lesion borders, where damaged tissues could coexist with healthy tissues (PVE), and whole structures, where doubts are due to MRI unspecific nature for MS.

Fig.2 reports a FLAIR image example with the corresponding binary consensus and the proposed ternary consensus. Uncertainty is in yellow in the ternary consensus, the last used as ground truth to train our framework in reaching a ternary classification.

3.3 CNN architecture

Being the problem at hand the classification of 2D slices of a FLAIR brain volume into the three classes, Background, Uncertainty and Lesion, in this work we use the U-Net 2D architecture [39] depicted in Figure 3, being U-nets specifically designed for these tasks.

Compared to the traditional U-net architecture, we insert a batch normalization layer in each block to mitigate the effects of the gradient amplification [42] in the regions surrounding the lesions, though with a relevant increase of computational costs (about 30%).

To optimize the number of blocks, n , we have performed preliminary training, with $n \in \{3, 4, 5\}$. We have not gone outside this set because for $n = 5$ the U-Net started to overfit, even when using high values of L_2 -Regularization, and for $n = 2$ a dramatic drop of performance occurred. With $n = 4$, the problems

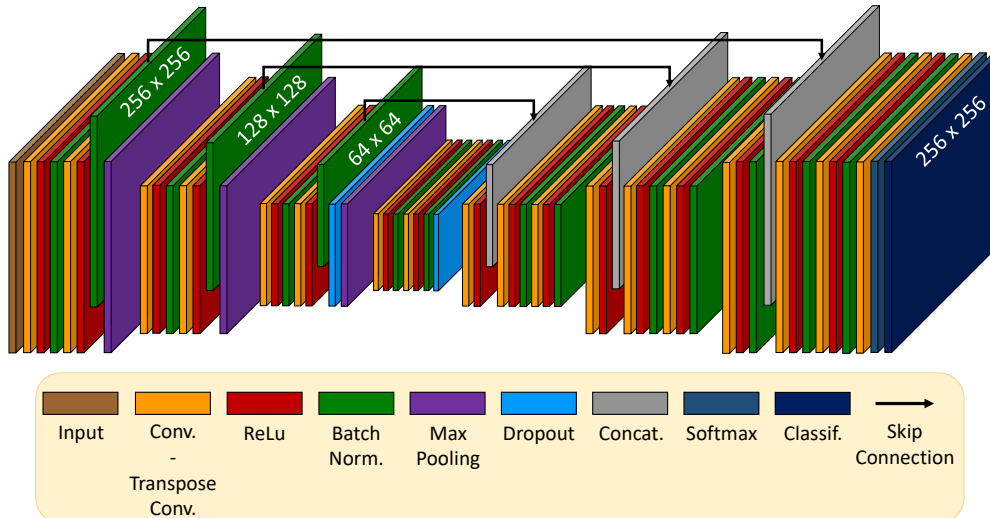


Figure 3: The used U-net "D" architecture. The architecture is the same for 6 classifiers, though they have been trained separately.

related to overfitting have disappeared and the performance was good but some redundancy remained. For this reason, we have trained the CNN with $n = 3$ and verified that redundancy was greatly reduced and training converged faster than for $n = 4$: hence, $n = 3$ is the number of selected blocks and used thereafter.

3.4 Loss function and process optimization

The architecture we use has to solve a three class automatic annotation, for which a Multi-label Cross Entropy Loss Function is necessary, defined as follows:

$$loss = \frac{1}{N} \sum_{n=1}^N \sum_{i=1}^K (T_{ni} \log(Y_{ni}) + (1 - T_{ni}) \log(1 - Y_{ni})) \quad (1)$$

where N and K are the numbers of observations and classes, respectively.

The use of three classes, besides the problem stabilization (the presence of Uncertainty gives better confidence in defining both Lesion and Background), allows also to consider another important aspect. Indeed, we can optimize two CNN, sharing the same architecture and the same loss function (Eq.1), but with a different learning focuses: Lesion and Background. The Uncertainty is used as a sort of "buffer class". In the case of a binary classification this would not have been possible: the optimization of one would automatically lead to the optimization of the other (what is not Lesion is Background and vice-versa). The usage of the Uncertainty gave to both CNN a new choice to break that constraint.

To achieve faster training and better performance, in this work the training process of each CNN is controlled by the following hyperparameters [44, 61]:

1. **Starting Learning Rate:** it is related to the data set and to the type of neural network.
2. **L2-Regularization:** it prevents overfitting.
3. **Class balancing:** it optimizes the amplification factor for the represented classes and improves training. Here we have three classes, hence two weights are sufficient (the Lesion weight and the Background one).

Of the above, the first two are standard for CNN, while Class balancing is specific for our CNN because it helps to differentiate the path of optimization.

The selected hyperparameters are automatically optimized through a Bayesian approach [44] applied to the following optimization problem:

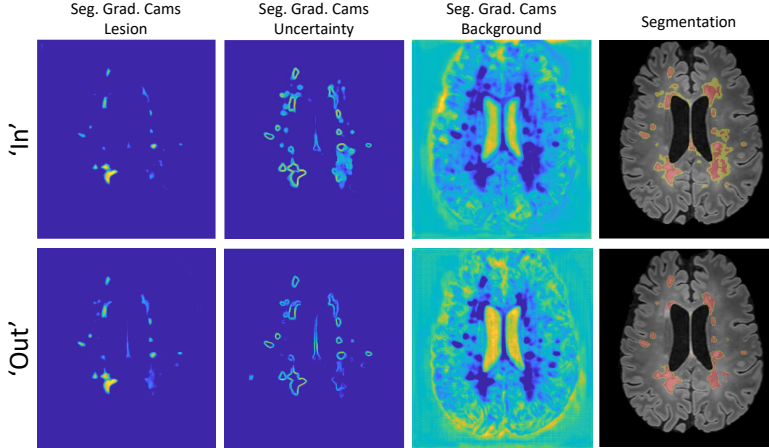


Figure 4: Grad-cam representation for an axial sample image for both CNN, Lesions from inside (In) and from outside (Out), respectively. Grad-cams are shown for the three classes, Lesion (first column), Uncertainty (second column) and Background (third column). The fourth column shows the resulting classification.

$$x^* = \operatorname{argmin}_{x \in X} f(x) \quad (2)$$

where X is the domain of x , $f(x)$ represents an objective function to be minimized and x^* is the hyperparameter setting that yields the optimal value of $f(x)$.

In this work $f(x)$ is defined as

$$f(x) = 1 - IoU(x) \quad (3)$$

where IoU is the Intersection over Union score [13] defined in Section 4.

For the two CNN used therein, the IoU is calculated on Lesion for the first and on Background for the second.

The hyperparameter settings for the optimized CNN in each direction are different and justify different training paths for the CNN and different points of convergence for each of them. Figure 4 shows the different behaviour of the two CNN in the segmentation grad-cams of a sample image, for the axial direction. The CNN optimized for Lesion, tends to enlarge Lesion and Uncertainty with respect to the CNN optimized for Background, which surrounds lesions from outside.

3.5 Ensemble Classification

It is well known that ensemble classifiers often perform better and more robustly than their single components [48, 57]. For classification, we use 2D slices of the whole volume, with specific CNN trained separately for Lesion and Background, each for axial, radial and sagittal orientations, respectively. In this way, we avoid that a particular orientation could be favourable to lesions or to the classifier. Further, it serves to ensure 3D continuity and to consider the context of lesions in the surrounding environment.

We obtain a set of 6 classifiers, whose classification has to be merged to produce a single output resembling the reasoning of the radiologists: though 3D FLAIR data are collected following sagittal planes to account for clinical/physical issues, radiologists often use axial images for data interpretation and the other orientations for confirmation [16, 49]. Accordingly, we prefer axial classifications and use coronal and sagittal output for confirmation.

Regarding axial classifications, since each of the two CNN referring to the same direction operates in the same scenario but with different focuses, they collect specific information where reasoning is specific. Since both specific contributions are important, besides common findings, a Union operation between the two classifications is required. This is in accordance with the double reading procedure followed by radiologists [17].

However, being the classified volume a three values data set, the Union does not correspond to the classic binary union operation. In our case, the Lesion is privileged, then comes the Uncertainty and, finally, the Background. In fact, a voxel is classified as part of a lesion if at least one of the two

classifications considers it as a lesion; elsewhere, if at least one of the two classifications considers it as uncertain, it is classified as Uncertainty, elsewhere, it is considered as Background.

After Union operation, false positives are more present than in each single classifier: their number is reduced by using the majority vote between the other 4 classifications (two coronal and 2 sagittal, being the comparison performed along axial planes). In fact, for each voxel the class is maintained if at least two of the other classifiers confirm it, elsewhere it is downgraded by one (a potential Lesion becomes Uncertainty, a potential Uncertainty becomes Background): a double step is not allowed. This means that first a decision is made on the Lesion and, then, on the Uncertainty by using the data set resulting from the application of the process to the Lesion.

The ensemble of different classifiers is justified both by the fact that the Union has to join common information, as well as specific information from each of the two axial classifiers, and because each potentially positive voxel needs confirmation from the coronal and sagittal classifiers (in this case, also 3D spatial information is considered). We have preferred to resemble the usual procedure used by radiologists and to rely on the usual benefits of using an ensemble classifier.

In the proposed automatic pipeline, we have copied the human behavior by privileging axial sections with respect to the others, but we have also performed trials regarding the preference of the other orientations in the fusion process and the results, not shown, confirm that the axial preference gives the best results, closely followed by the coronal and, at a great distance, by the sagittal, though this is the direction used for 3D FLAIR data collection. This could be explained, at least partially, by the fact that axial and coronal slices show highly symmetrical shape both regarding brain anatomy and lesion shapes, also across subjects, thus making the learning process easier than for sagittal slices. In sagittal directions symmetry is absent and a huge variation of the image content could correspond to a little rotation of the head.

4 Performance Parameters

In the binary classification problem the voxels can be positive (P, or Lesion) or negative (N or Background). In a ternary ground-truth, P represents the voxels of the class we are considering at present (Lesion or Uncertainty), while N represents the negative voxels (those of the other two classes). According to this definition, the same rules apply for each rater (with respect to the class considered at present): TP are the true positive voxels, TN are the true negative voxels, FP are the false positive voxels and FN are the false negative voxels. Referring to a given class, a classified voxel can be just in one of the states TP , TN , FP and FN .

As far as we need an exhaustive comparison between all the raters involved therein (artificial, single humans and ground truth), and being a unique performance parameter unavailable, we define and calculate all the mostly known scores and metrics. Despite of a certain redundancy, we use the rule of thumb that it is better to over-describe the results than under-describe them in order to highlight any potential sorts of errors the model could make and to avoid that masking these errors could result in an advantage for the model itself. In what follows, we define all the used parameters by separating scores, defined in $[0, 1]$ and whose ideal value is 1, from metrics, defined in $[0, \infty)$ and whose best value is 0. The two groups are distinguished for graphical purposes. For more details about the reported metrics, please refer to [11–13].

4.1 Scores (convergent to 1)

Sensitivity (also called recall or true positive rate) is defined as:

$$SENS = \frac{TP}{TP + FN} \quad (4)$$

$SENS$ measures the portion of positive voxels that are correctly identified. We also distinguish an object sensitivity, $OSENS$, defined as:

$$OSENS = \frac{TP_o}{TP_o + FN_o} \quad (5)$$

in which the prefix O and the subscript o indicate we are referring to whole objects and not to single voxels. An object is considered as TP if the intersection with the corresponding object in the ground-truth is not empty.

Specificity ($SPEC$) is defined as:

$$SPEC = \frac{TN}{TN + FP} \quad (6)$$

SPEC represents the portion of negative voxels N that have been correctly identified. For the treated case, where classes are strongly unbalanced, *SPEC* is biased by the fact that most of the image surface is covered by background (unbalancing).

For the accuracy (*ACC*), we use the following normalized definition to reduce unbalancing effects:

$$ACC = \left(\frac{TP}{TP + FN} + \frac{TN}{TN + FP} \right) / 2 \quad (7)$$

Positive Predicted Value (*PPV*), also called Precision, is defined as:

$$PPV = \frac{TP}{TP + FP} \quad (8)$$

PPV represents the portion of voxels identified as positives which are really positives (*TP*).

As for *OSENS*, we define an object-based *PPV*, *OPPV* as follows:

$$OPPV = \frac{TP_o}{TP_o + FP_o} \quad (9)$$

in which the prefix O and the subscript o indicate we are referring to whole objects not to single objects, as above.

Dice score, also called Sorensen–Dice coefficient, is defined as:

$$Dice = \frac{2 * TP}{2 * TP + FP + FN} \quad (10)$$

Dice measures the similarity between two data sets. This index is widely used in AI for the validation of image segmentation algorithms.

Image Dice score uses the same equation of *Dice* but, while *Dice* is calculated on the whole data set, *Image Dice* is applied on each image separately and the results are averaged on the number of images. *Image Dice* allows to the so called per-image evaluation [12]. Per-image evaluations are important because they tend to highlight the local behaviour. For our comparisons, we calculate both *Dice* and *Image Dice*.

A score similar to *Dice* is the Intersection Over Union (*IoU*):

$$IoU = \frac{TP}{TP + FP + FN} \quad (11)$$

where the difference is in the weight of *TP*.

The *F1* Score (calculated for whole objects and not for single voxels) is defined as:

$$F1 = 2 * \frac{OSENS * OPPV}{OSENS + OPPV} \quad (12)$$

where *OSENS* and *OPPV* are defined above.

The Boundary *F1* score (*BF*) is a per-image version of *F1* score.

Pearson Correlation Coefficient (*PCC*), between two data sets A and B , is defined as:

$$PCC(A, B) = \frac{cov(A, B)}{\sigma_A * \sigma_B} \quad (13)$$

where $cov(A, B)$ is the covariance of A and B and σ_A and σ_B are the standard deviation of A and B , respectively. *PCC* ranges in the interval $[-1, 1]$ and a negative value of *PCC* indicates a similarity of the object A with the negative version of the object B .

4.2 Metrics (convergent to 0)

The following metrics are those used in the present manuscript in which the ideal value is 0.

Extra Fraction (EF), is defined as:

$$EF = \frac{FP}{TP + FN} \quad (14)$$

Detection error rate (DER) is defined as:

$$DER = \frac{DE}{MTA} \quad (15)$$

where the detection error DE is calculated as the sum of the voxels of connected regions wrongly marked as positive by the rater and the mean total area MTA is defined as the average between the number of positive voxels from the rater and the ground-truth. DER measures the disagreement in detecting the same regions between a rater under and the ground-truth.

Outline Error Rate (OER) is defined as:

$$OER = \frac{OE}{MTA} \quad (16)$$

where OE is the outline error calculated as the difference between the number of voxels of the union and that of the intersection between the positive connected regions of both the rater and the ground-truth. OER measures the disagreement in outlining the same objects between a rater and the ground truth.

False Detection Ratio (FDE) is defined as:

$$FDE = \frac{FP}{P} \quad (17)$$

Relative Area Error (RAE) is defined as:

$$RAE = \frac{TP + FP - P}{P} \quad (18)$$

Hausdorff Distance (HD) between two objects A and B is defined as:

$$HD(A, B) = \max(h(A, B), h(B, A)) \quad (19)$$

where $h(A, B)$ is:

$$h(A, B) = \max_{a \in A} \min_{b \in B} \| a - b \| \quad (20)$$

HD measures how far two subsets are from each other. In other words, two sets are close with respect to HD if every point of one set is close to a certain point of the other set.

Euclidean Distance (ED) between two objects A and B is defined as:

$$ED(A, B) = \max(d(A, B), d(B, A)) \quad (21)$$

where $d(A, B)$ is defined as:

$$d(A, B) = \frac{1}{N} \sum_{a \in A} \min_{b \in B} \| a - b \| \quad (22)$$

Surface Distance (SD) is defined as:

$$SD = \frac{\sum_{i \in A_S} d(x_i, G_S) + \sum_{j \in G_S} d(x_j, A_S)}{N_A + N_G} \quad (23)$$

where A_S and G_S are two segmentations (one is the rater segmentation and the other is the ground truth), d denotes the minimal ED between voxels on both surfaces, while N_A and N_G denote the number of points of each surface.

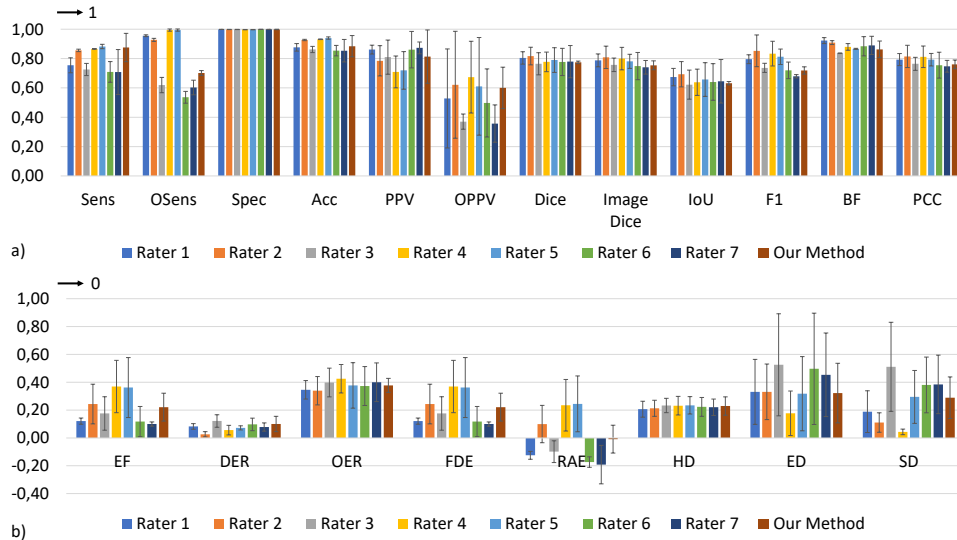


Figure 5: Comparison between the raters and the ground truth, performed on the Lesion class. The reported metrics are separated in those whose ideal value is 1 (a) and those whose ideal value is 0 (b). Average and standard deviation are reported. Euclidean, Hausdorff and Surface distances are shown in cm units.

5 Results and Discussion

The proposed framework has been trained, validated and tested on the ternary ground-truth defined above. As far as the ground-truth maintains unaltered Lesion of the original binary ground-truth, we guarantee a direct comparison with human raters and, at the same time, with already existing automated methods. Regarding the segmented Uncertainty, a comparison is possible just with respect to the ternary ground-truth, since for the human raters Uncertainty is unavailable.

The evaluation of the proposed framework and of the human radiologists, with respect both to the ground-truth and to each-other, is performed by applying the cross-validation approach defined in Subsection 3.1. Average and standard deviation values are calculated for the evaluation parameters defined in Section 4 and divided in two groups: those whose ideal value is 1 and those whose ideal value is 0.

The first results, reported in Fig 5, are those between the raters and the ground-truth performed on the Lesion class. This is also an indirect comparison, through the ground-truth, between the proposed framework and the human raters. For a better overview, the mean values are also shown in Fig. 6 by using a radar visualization: they confirm that the behaviour of the proposed method is inside the inter-rater variability.

As it can be observed, our framework is never the best or the worst, for at least one of the metrics, as instead occurs for human raters. This can be explained, at least partially, by the fact that it has been trained with the consensus that, for its nature, tends to average pros and cons of the raters from which it has been derived.

A Wilcoxon signed-rank test of the vectors of metric values confirms, with a significance level of 0.01, that there is no significant difference between the behaviour of our method and that of the 7 human raters, with respect to the ground-truth, on the Lesion class. This means that, if data are shown without labels, it would be impossible to recognize the automated rater from humans.

As far as the lesion size could greatly affect the performance of the classification [11] and the previously reported results are averaged with respect to the lesion volume, we repeat the comparison by changing the lesion volume. To this aim, we consider all the lesions separately and the calculations are performed lesion by lesion, by maintaining separated also the lesions of the same volume. In this way we can: 1) visualize potential outliers; 2) represent lesion density; 3) avoid local averaging that could mask specific contributions. The results, reported just for the most commonly used evaluation parameters [11], are shown in Fig. 7.

It is confirmed the analogy of behavior between the proposed framework and the 7 human raters, though for some volumes our framework has exhibited results close to the borders of oscillation of the 7 human raters. Indeed, a greater dispersion can be observed for F1-score and a relatively high average

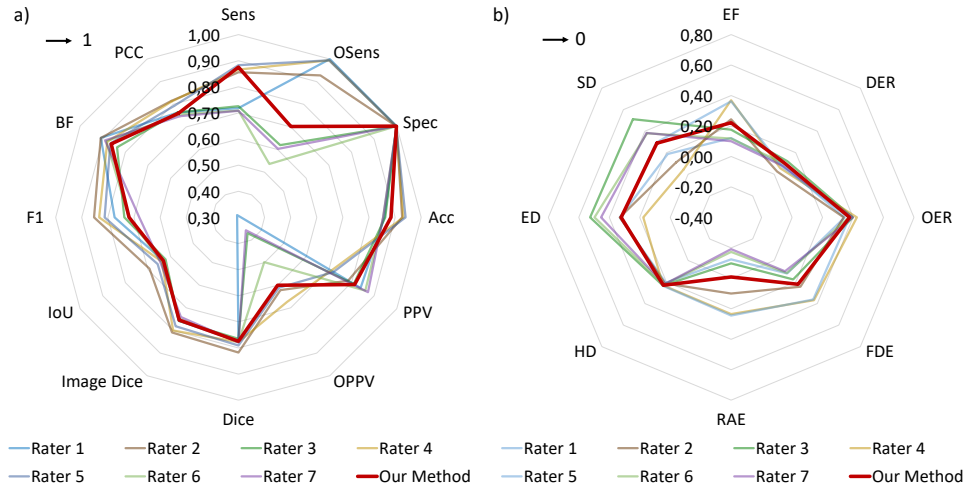


Figure 6: Comparison between raters in the same conditions of Fig. 5. For graphic purposes, only the average values are reported and the line of the proposed framework (red) is highlighted with respect to the others.

value is observable for SD , though in line with that of some human raters.

The above good results are not sufficient alone to state that our framework behaves like human raters because the comparison is through the ground-truth. In other words, our framework could be at the same 'distance' as the human raters are from the ground-truth, but from opposite sides. For this reason, a direct comparison is necessary to finally confirm the similarity between the proposed framework and the human raters. To this aim, we perform the experiment of comparing all the raters to each other by considering ground-truth all of them, including our framework, in rotation. Results, for the most frequently used metrics, are reported in Fig. 8.

These results confirm that the proposed framework behaviour does not differ from that of the other human raters and that it is not polarized toward a specific rater or toward the ground-truth. Moreover, as other Authors have highlighted [20], results show similarities among some human raters (R4 with R5 and R6 with R7). Fortunately, results also confirm that the ground-truth is not biased by the similarity between some raters, and that it maintains a "human" behaviour, being it very close to the raters R1 and R2. This is a fundamental aspect because it means that all the people who are attempting to train automated systems with respect to the ground-truth, including ourselves, are not following a "chimera" to which, paradoxically, the closer we get, the more we move away from the proper objective.

A visual overview of the behaviour of the proposed framework in the whole process of identification/segmentation, both for Lesion and for Uncertainty, with respect to the ternary ground truth, is shown in Fig. 9. The ternary ground-truth is reported on the left side, the corresponding segmentation obtained with the proposed framework is presented on the right side, for the same subject and slices. Both for Lesion and Uncertainty, the proposed framework selects more than necessary (FP are evident). Interestingly, FN are almost absent from the segmented volume. The other interesting property shown by the proposed framework is the good spatial continuity of the lesion structures in the 3D model of Lesion (upper right panel, where Lesion is red colored while Uncertainty is yellow colored).

To complete our discussion, we compare the proposed framework with recently proposed automated strategies. To this aim, Table 1 contains this indirect comparison on the metrics calculated for at least one of the other methods. The necessary condition for a method to be considered in Table 1 is to have been trained, validated and tested on the MSSEG data set. In this way, we can ensure that the comparison is homogeneous and performed on the same conditions of that obtained with respect to the 7 human raters.

Though a global ranking is difficult, data reported in Table 1 are clear: the proposed framework is the most stable with respect to different metrics and it generally outperforms the other methods, including those using multiple imaging. This could have an interesting implication: FLAIR would contain sufficient information, not only necessary, to identify and segment all MS lesions occurring in the WM. Potentially positive consequences are: a) due to the huge variability of MRI and of its modalities, the usage of a single modality could increase the performance, above using multiple modalities, because it could greatly contribute to stabilize automatic identification/classification; b) the acquisition time and stress for the

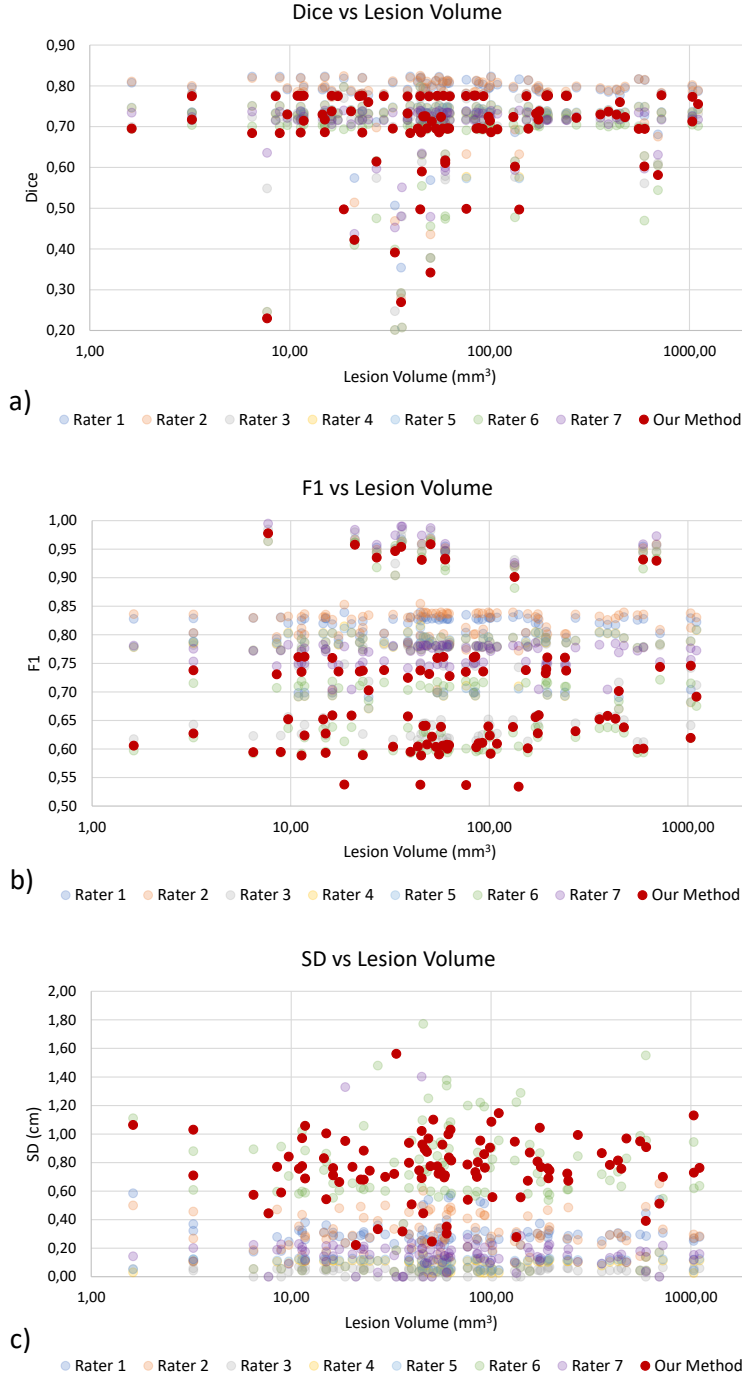


Figure 7: Dice score (a), F1-score (b) and Surface Distance (c), calculated for each lesion and shown with respect to the lesion volume for the human raters and the proposed framework. To improve readability; lesion volume is represented in logarithmic scale; framework’s values (red) are highlighted.

patient can be reduced.

An important aspect that has determined the outstanding performance of the proposed framework is the use of the ternary ground-truth. Indeed, Fig. 10 shows the average performance results when the proposed framework is trained without the Uncertainty (on the binary consensus) as compared to those obtained when trained on the ternary consensus. The ensemble method trained without the Uncertainty outperforms similar automated strategies (team fusion in [11]), though it is still far from humans: the step which places the proposed framework among humans is the inclusion in the pipeline of the class Uncertainty.

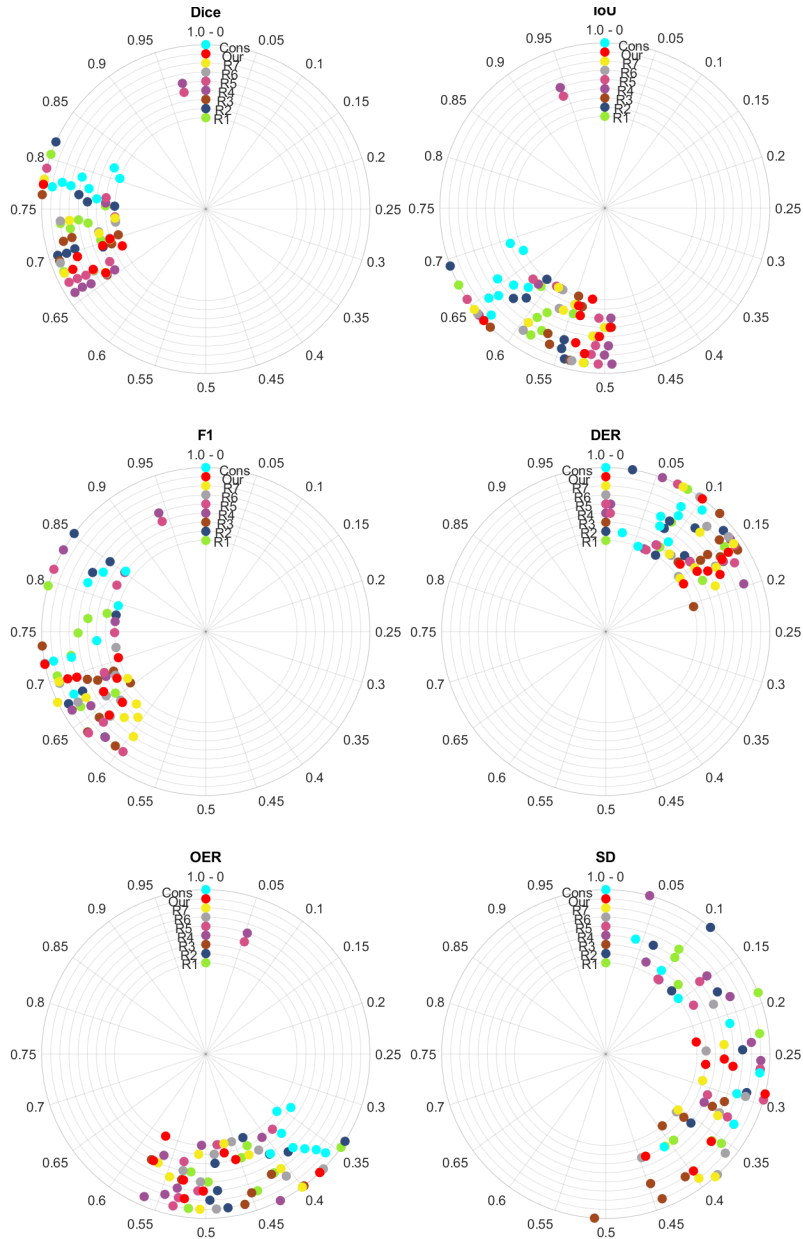


Figure 8: Comparison between all the raters with respect to each other, including our framework and consensus, each alternately considered as the ground-truth. For readability purposes, only some metrics are reported. In this representation, placing together metrics converging to 1 and to 0, the angular position indicates the metric value: clock wise versus for metrics converging to 1, anti-clock wise versus for metrics converging to 0. Radial information is only used to separate the current ground-truth raters. Ground-truth raters have colored bullets placed on the vertical line.

This is in line with what reported in [20]: the framework learns better what is surely Lesion, what is surely Background and uses Uncertainty for doubts, as a buffer class. Indeed, the polarized and ambiguous classification of doubtful voxels, sometimes as Lesion and others as Background, disorients any automated strategy and deviates it from the human reasoning.

6 Conclusion and future work

An automated framework for the identification/segmentation of MS lesions from FLAIR MRI images has been presented. We have demonstrated that traditional CNN architectures, if placed in a context emulating the procedures of human specialists, could effectively behave like a human expert. The strength

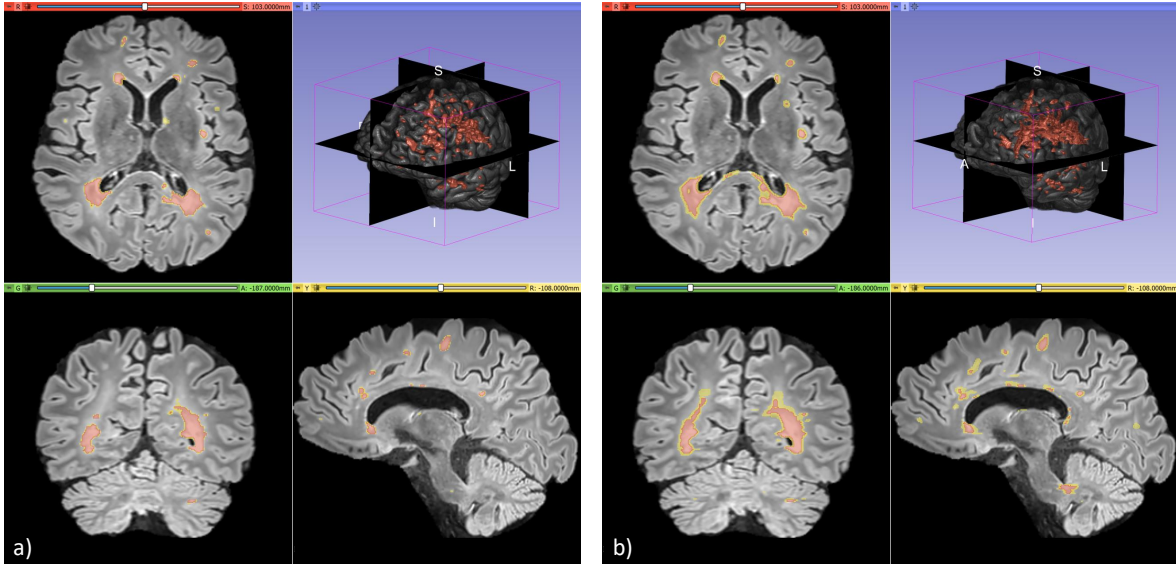


Figure 9: Comparison between the ternary ground truth (left) and the proposed automated framework (right). Lesion is red and Uncertainty is yellow. For readability purposes, the upper right panel of each side shows just the healthy brain and Lesion in 3D.

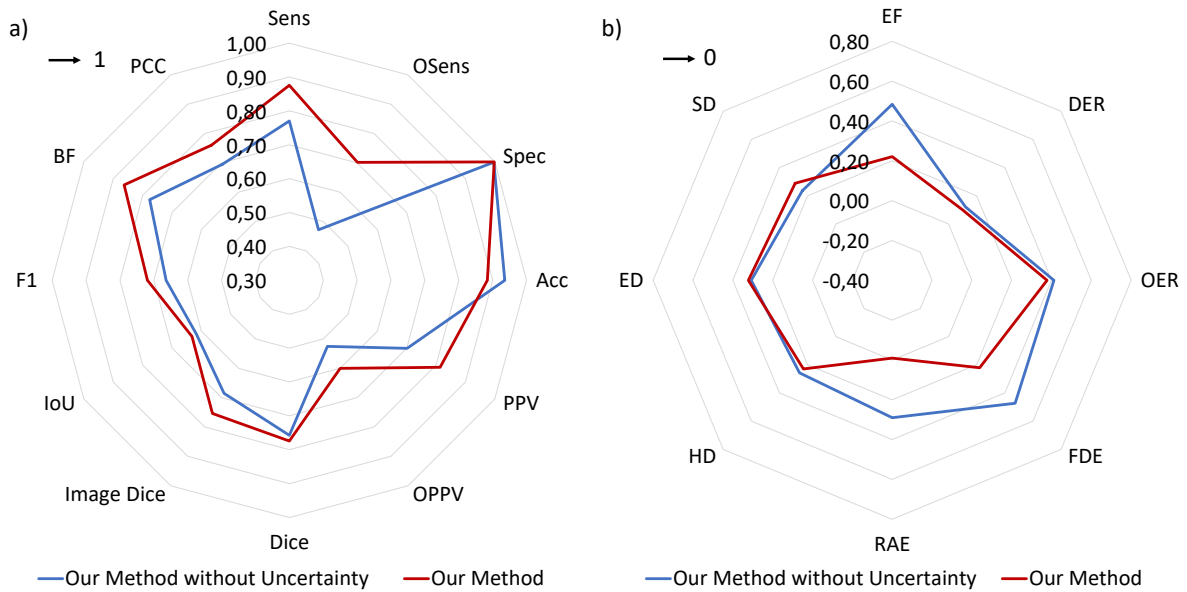


Figure 10: The proposed method when trained without and with Uncertainty, compared both on metrics whose ideal value is 1 (a) and for metrics whose ideal value is 0 (b).

points of the proposed framework are the following: 1) to train the system to recognize both the lesions as they are and with respect to the environment they are immersed in, thus allowing to incorporate also a sort of meta-information regarding the environment where MS lesions mostly occur; 2) to resemble radiologists in consulting axial slices to discover potential lesions and to check radial and sagittal slices for confirmation, as well as to maintain 3D continuity to their findings; 3) to use an ensemble classification that usually performs better than its components; 4) to use an artificially generated Uncertainty class to improve the performance of an automated strategy and to make it more similar to the human reasoning; 5) to operate just on FLAIR images.

Results have shown that the proposed framework resembles human raters both in behaviour and in performance, when compared with the MSSEG consensus on Lesion. Indeed, Wilcoxon statistical test has assessed the framework ability to exhibit a behaviour that is equivalent to, or indistinguishable

Table 1: Comparison between our framework and the state of the art methods. Just averages are reported and the symbol '-' is for unavailable data. For the state of the art strategies, the performance values are those reported in the original manuscripts, while for Team Fusion (TF) the metrics are those reported in [11].

Method	MRI mod.	Sens	OSens	TPR	Acc	PPV	OPPV	Dice	F1	SD
TS [11]	FLAIR, PD, T2 T1, G-E T1	0.71	0.60	0.99	-	0.65	0.53	0.64	0.50	0.91
[19]	FLAIR, PD, T2 T1, G-E T1	0.65	-	0.86	0.97	-	-	0.76	-	-
[51]	FLAIR, T1	0.55	-	-	-	-	0.79	0.63	-	-
[3]	FLAIR, PD T1, G-E T1	0.76	-	-	-	-	-	0.82	-	-
[34]	FLAIR, T1, T2	-	-	-	-	-	-	0.76	0.59	-
Our	FLAIR	0.88	0.77	0.98	0.88	0.81	0.81	0.77	0.72	0.27

from, that of a human rater. Furthermore, the proposed framework outperforms the state of the art strategies which have been trained, validated and tested on the MSSEG data set. Finally, the usage of the uncertainty during training has greatly improved the performance of the framework.

In a recent report [24], the JASON Advisory Group has identified several key recommendations for advancing computation technology into routine clinical practice. One of them is that new technologies should address a significant clinical need, be practical in use and reduce medical system costs. The demonstration that a better performance is possible by including some concepts (Uncertainty and Ensemble) to enrich traditional CNN architectures goes in the direction of the above recommendations.

Future directions of exploration will be: 1) an accurate definition of "Uncertainty" and a deep study of its role in the intrinsically uncertain decision-making process; 2) the use of specific pre-processing strategy for the FLAIR images to further improve the robustness of the method with respect to MRI and MRI scanners variability; 3) how multiple imaging could affect the classification performance; 4) how the use of a different loss function could better deal the unbalancing problem 5) to study a "soft" consensus based on a single class (lesion) with different probability values to reduce problem complexity and to explore a "soft" loss function; 6) to test the proposed framework to identify/segment also cortical lesions and for longitudinal studies (temporal evolution of the disease); 7) to explore specific pre-processing strategies to make all the used modalities robust with respect to MRI and MRI scanners; 8) to study the role of additional meta-information in improving lesion identification.

Acknowledgments

The Authors wish to thank Dr Maria Silvia Marottoli for her contribution to the improvement of the manuscript.

References

- [1] *MSSEG Challenge Proceedings: Multiple Sclerosis Lesions Segmentation Challenge Using a Data Management and Processing Infrastructure*, Athènes, Greece, 2016.
- [2] H. M. Rehan Afzal, Suhuai Luo, Saadallah Ramadan, and Jeannette Lechner-Scott. The emerging role of artificial intelligence in multiple sclerosis imaging. *Multiple Sclerosis Journal*, page 135245852096629, October 2020.
- [3] Ali Alijamaat, Alireza NikravanShalmani, and Peyman Bayat. Multiple sclerosis lesion segmentation from brain mri using u-net based on wavelet pooling. *International Journal of Computer Assisted Radiology and Surgery*, pages 1–9, 2021.

- [4] Roohallah Alizadehsani, Mohamad Roshanzamir, Sadiq Hussain, Abbas Khosravi, Afsaneh Koohestani, Mohammad Hossein Zangoeei, Moloud Abdar, Adham Beykikhoshk, Afshin Shoeibi, Assef Zare, Maryam Panahiazar, Saeid Nahavandi, Dipti Srinivasan, Amir F. Atiya, and U. Rajendra Acharya. Handling of uncertainty in medical data using machine learning and probability theory techniques: a review of 30 years (1991–2020). *Annals of Operations Research*, March 2021.
- [5] Shahab Aslani, M. Dayan, L. Storelli, M. Filippi, Vittorio Murino, M. Rocca, and Diego Sona. Multi-branch convolutional neural network for multiple sclerosis lesion segmentation. *NeuroImage*, 196:1–15, 2019.
- [6] L. S. Aït-Ali, S. Prima, P. Hellier, B. Carsin, G. Edan, and C. Barillot. STREM: A robust multidimensional parametric method to segment MS lesions in MRI. In *Lecture Notes in Computer Science*, pages 409–416. Springer Berlin Heidelberg, 2005.
- [7] T. Brosch, L. Y. W. Tang, Y. Yoo, D. K. B. Li, A. Traboulsee, and R. Tam. Deep 3d convolutional encoder networks with shortcuts for multiscale feature integration applied to multiple sclerosis lesion segmentation. *IEEE Transactions on Medical Imaging*, 35(5):1229–1239, 2016.
- [8] Mariano Cabezas, Arnau Oliver, Sergi Valverde, Brigitte Beltran, Jordi Freixenet, Joan C. Vilanova, Lluís Ramió-Torrentà, Àlex Rovira, and Xavier Lladó. BOOST: A supervised approach for multiple sclerosis lesion segmentation. *Journal of Neuroscience Methods*, 237:108–117, nov 2014.
- [9] Aaron Carass, Snehashis Roy, Amod Jog, Jennifer L. Cuzzocreo, Elizabeth Magrath, Adrian Gherman, Julia Button, James Nguyen, Ferran Prados, Carole H. Sudre, Manuel Jorge Cardoso, Niamh Cawley, Olga Ciccarelli, Claudia A.M. Wheeler-Kingshott, Sébastien Ourselin, Laurence Catanese, Hrishikesh Deshpande, Pierre Maurel, Olivier Commowick, Christian Barillot, Xavier Tomas-Fernandez, Simon K. Warfield, Suthirth Vaidya, Abhijith Chunduru, Ramanathan Muthuganapathy, Ganapathy Krishnamurthi, Andrew Jesson, Tal Arbel, Oskar Maier, Heinz Handels, Leonardo O. IHEME, Devrim Unay, Saurabh Jain, Diana M. Sima, Dirk Smeets, Mohsen Ghafoorian, Bram Platel, Ariel Birenbaum, Hayit Greenspan, Pierre-Louis Bazin, Peter A. Calabresi, Ciprian M. Crainiceanu, Lotta M. Ellingsen, Daniel S. Reich, Jerry L. Prince, and Dzung L. Pham. Longitudinal multiple sclerosis lesion segmentation: Resource and challenge. *NeuroImage*, 148:77–102, mar 2017.
- [10] Alexandre Carré, Guillaume Klausner, Myriam Edjlali, Marvin Lerousseau, Jade Briend-Diop, Roger Sun, Samy Ammari, Sylvain Reuzé, Emilie Alvarez Andres, Théo Estienne, Stéphane Niyoteka, Enzo Battistella, Maria Vakalopoulou, Frédéric Dhermain, Nikos Paragios, Eric Deutsch, Catherine Oppenheim, Johan Pallud, and Charlotte Robert. Standardization of brain MR images across machines and protocols: bridging the gap for MRI-based radiomics. *Scientific Reports*, 10(1), jul 2020.
- [11] Olivier Commowick, Audrey Istace, Michaël Kain, Baptiste Laurent, Florent Leray, Mathieu Simon, Sorina Camarasu Pop, Pascal Girard, Roxana Améli, Jean-Christophe Ferré, Anne Kerbrat, Thomas Tourdias, Frédéric Cervenansky, Tristan Glatard, Jérémy Beaumont, Senan Doyle, Florence Forbes, Jesse Knight, April Khademi, Amirreza Mahbod, Chunliang Wang, Richard McKinley, Franca Wagner, John Muschelli, Elizabeth Sweeney, Eloy Roura, Xavier Lladó, Michel M. Santos, Wellington P. Santos, Abel G. Silva-Filho, Xavier Tomas-Fernandez, Hélène Urien, Isabelle Bloch, Sergi Valverde, Mariano Cabezas, Francisco Javier Vera-Olmos, Norberto Malpica, Charles Guttmann, Sandra Vukusic, Gilles Edan, Michel Dojat, Martin Styner, Simon K. Warfield, François Cotton, and Christian Barillot. Objective evaluation of multiple sclerosis lesion segmentation using a data management and processing infrastructure. *Scientific Reports*, 8(1), sep 2018.
- [12] Gabriela Csurka, Diane Larlus, Florent Perronnin, and France Meylan. What is a good evaluation measure for semantic segmentation?. In *Bmvc*, volume 27, pages 10–5244, 2013.
- [13] Antonios Danelakis, Theoharis Theoharis, and Dimitrios A. Verganelakis. Survey of automated multiple sclerosis lesion segmentation techniques on magnetic resonance imaging. *Computerized Medical Imaging and Graphics*, 70:83 – 100, 2018. ISSN 0895-6111.
- [14] Randa ElSebely, Ahmed Hassan Yousef, Ashraf A Salem, and Bassem Abdullah. Automatic segmentation of multiple sclerosis lesions in brain mr images using ensemble machine learning. In *2021 International Mobile, Intelligent, and Ubiquitous Computing Conference (MIUCC)*, pages 28–33. IEEE, 2021.

- [15] Alexandre Fenneteau, Pascal Bourdon, David Helbert, Christine Fernandez-Maloigne, Christophe Habas, and Remy Guillevin. Learning a cnn on multiple sclerosis lesion segmentation with self-supervision. In *International Symposium on Electronic Imaging 2020 3D Measurement and Data Processing*, pages 1–8. HAL open science, 2020.
- [16] Massimo Filippi, Paolo Preziosa, Brenda L Banwell, Frederik Barkhof, Olga Ciccarelli, Nicola De Stefano, Jeroen J G Geurts, Friedemann Paul, Daniel S Reich, Ahmed T Toosy, Anthony Traboulsee, Mike P Wattjes, Tarek A Yousry, Achim Gass, Catherine Lubetzki, Brian G Weinschenker, and Maria A Rocca. Assessment of lesions on magnetic resonance imaging in multiple sclerosis: practical guidelines. *Brain*, 142(7):1858–1875, 06 2019. ISSN 0006-8950.
- [17] Håkan Geijer and Mats Geijer. Added value of double reading in diagnostic radiology, a systematic review. *Insights into Imaging*, 9(3):287–301, March 2018.
- [18] Ezequiel Geremia, Olivier Clatz, Bjoern H. Menze, Ender Konukoglu, Antonio Criminisi, and Nicholas Ayache. Spatial decision forests for MS lesion segmentation in multi-channel magnetic resonance images. *NeuroImage*, 57(2):378–390, July 2011.
- [19] Palash Ghosal, Pindi Krishna Chandra Prasad, and Debashis Nandi. A light weighted deep learning framework for multiple sclerosis lesion segmentation. In *2019 Fifth International Conference on Image Information Processing (ICIIP)*, pages 526–531. IEEE, 2019.
- [20] Charley Gros, Andreeanne Lemay, and Julien Cohen-Adad. Softseg: Advantages of soft versus binary training for image segmentation. *Medical Image Analysis*, 71:102038, 2021.
- [21] Nicolas Guizard, Pierrick Coupé, Vladimir S. Fonov, Jose V. Manjón, Douglas L. Arnold, and D. Louis Collins. Rotation-invariant multi-contrast non-local means for MS lesion segmentation. *NeuroImage: Clinical*, 8:376–389, 2015.
- [22] S. R. Hashemi, S. S. Mohseni Salehi, D. Erdogmus, S. P. Prabhu, S. K. Warfield, and A. Gholipour. Asymmetric loss functions and deep densely-connected networks for highly-imbalanced medical image segmentation: Application to multiple sclerosis lesion detection. *IEEE Access*, 7:1721–1735, 2019.
- [23] Yi-Jie Huang, Qi Dou, Zi-Xian Wang, Li-Zhi Liu, Ying Jin, Chao-Feng Li, Lisheng Wang, Hao Chen, and Rui-Hua Xu. 3-d roi-aware u-net for accurate and efficient colorectal tumor segmentation. *IEEE Transactions on Cybernetics*, 51(11):5397–5408, 2021.
- [24] JASON. Artificial intelligence for health and health care. *JSR-17-Task-002*, 2017.
- [25] Guixia Kang, Beibei Hou, Yiyuan Ma, Fabrice Labeau, Zichen Su, et al. Acu-net: A 3d attention context u-net for multiple sclerosis lesion segmentation. In *ICASSP 2020-2020 IEEE International Conference on Acoustics, Speech and Signal Processing (ICASSP)*, pages 1384–1388. IEEE, 2020.
- [26] Z. Karimaghloo, M. Shah, S. J. Francis, D. L. Arnold, D. L. Collins, and T. Arbel. Automatic detection of gadolinium-enhancing multiple sclerosis lesions in brain mri using conditional random fields. *IEEE Transactions on Medical Imaging*, 31(6):1181–1194, 2012.
- [27] Eytan Kats, Jacob Goldberger, and Hayit Greenspan. Soft labeling by distilling anatomical knowledge for improved MS lesion segmentation. In *2019 IEEE 16th International Symposium on Biomedical Imaging (ISBI 2019)*. IEEE, apr 2019.
- [28] Amrita Kaur, Lakhwinder Kaur, and Ashima Singh. State-of-the-art segmentation techniques and future directions for multiple sclerosis brain lesions. *Archives of Computational Methods in Engineering*, feb 2020.
- [29] Chunfeng Lian, Mingxia Liu, Yongsheng Pan, and Dinggang Shen. Attention-guided hybrid network for dementia diagnosis with structural mr images. *IEEE Transactions on Cybernetics*, 52(4), 2022.
- [30] Geert Litjens, Thijs Kooi, Babak Ehteshami Bejnordi, Arnaud Arindra Adiyoso Setio, Francesco Ciompi, Mohsen Ghahfoorian, Jeroen A.W.M. van der Laak, Bram van Ginneken, and Clara I. Sánchez. A survey on deep learning in medical image analysis. *Medical Image Analysis*, 42:60–88, dec 2017.

- [31] Chenghao Liu, Xiangzhu Zeng, Kongming Liang, Yizhou Yu, and Chuyang Ye. Improved brain lesion segmentation with anatomical priors from healthy subjects. pages 186–195. Springer International Publishing, 2021.
- [32] Mingxia Liu, Jun Zhang, Chunfeng Lian, and Dinggang Shen. Weakly supervised deep learning for brain disease prognosis using mri and incomplete clinical scores. *IEEE Transactions on Cybernetics*, 50(7):3381–3392, 2020.
- [33] U. Macar, Enamundram Naga Karthik, Charley Gros, Andr’eanne Lemay, and Julien Cohen-Adad. Team neuropoly: Description of the pipelines for the miccai 2021 ms new lesions segmentation challenge. *ArXiv*, abs/2109.05409, 2021.
- [34] Richard McKinley, Rik Wepfer, Fabian Aschwanden, Lorenz Grunder, Raphaela Muri, Christian Rummel, Rajeev Verma, Christian Weisstanner, Mauricio Reyes, Anke Salmen, et al. Simultaneous lesion and brain segmentation in multiple sclerosis using deep neural networks. *Scientific reports*, 11(1):1–11, 2021.
- [35] F. Milletari, N. Navab, and S. Ahmadi. V-net: Fully convolutional neural networks for volumetric medical image segmentation. In *2016 Fourth International Conference on 3D Vision (3DV)*, pages 565–571, 2016.
- [36] Dong Nie, Li Wang, Ehsan Adeli, Cuijin Lao, Weili Lin, and Dinggang Shen. 3-d fully convolutional networks for multimodal isointense infant brain image segmentation. *IEEE Transactions on Cybernetics*, 49(3):1123–1136, 2019.
- [37] G. Placidi. *Mri: Essentials for innovative technologies (1st ed.)*, 2012.
- [38] Giuseppe Placidi, Luigi Cinque, Matteo Polsinelli, Alessandra Splendiani, and Emanuele Tomasino. Automatic framework for multiple sclerosis follow-up by magnetic resonance imaging for reducing contrast agents. In *Image Analysis and Processing – ICIAP 2019*, pages 367–378, Cham, 2019. Springer International Publishing.
- [39] Olaf Ronneberger, Philipp Fischer, and Thomas Brox. U-net: Convolutional networks for biomedical image segmentation. In Nassir Navab, Joachim Hornegger, William M. Wells, and Alejandro F. Frangi, editors, *Medical Image Computing and Computer-Assisted Intervention – MICCAI 2015*, pages 234–241, Cham, 2015. Springer International Publishing.
- [40] Francesco La Rosa, Mário João Fartaria, Tobias Kober, Jonas Richiardi, Cristina Granziera, Jean-Philippe Thiran, and Meritxell Bach Cuadra. Shallow vs deep learning architectures for white matter lesion segmentation in the early stages of multiple sclerosis. In *Brainlesion: Glioma, Multiple Sclerosis, Stroke and Traumatic Brain Injuries*, pages 142–151. Springer International Publishing, 2019.
- [41] Eloy Roura, Arnau Oliver, Mariano Cabezas, Sergi Valverde, Deborah Pareto, Joan C. Vilanova, Lluís Ramió-Torrentà, Àlex Rovira, and Xavier Lladó. A toolbox for multiple sclerosis lesion segmentation. *Neuroradiology*, 57(10):1031–1043, jul 2015.
- [42] Shibani Santurkar, Dimitris Tsipras, Andrew Ilyas, and Aleksander Madry. How does batch normalization help optimization? In *Proceedings of the 32nd International Conference on Neural Information Processing Systems*, NIPS’18, page 2488–2498, Red Hook, NY, USA, 2018. Curran Associates Inc.
- [43] Navid Shiee, Pierre-Louis Bazin, Arzu Ozturk, Daniel S. Reich, Peter A. Calabresi, and Dzung L. Pham. A topology-preserving approach to the segmentation of brain images with multiple sclerosis lesions. *NeuroImage*, 49(2):1524–1535, jan 2010.
- [44] Jasper Snoek, Hugo Larochelle, and Ryan P. Adams. Practical bayesian optimization of machine learning algorithms. In *Proceedings of the 25th International Conference on Neural Information Processing Systems - Volume 2*, NIPS’12, page 2951–2959, Red Hook, NY, USA, 2012. Curran Associates Inc.

- [45] Žiga Špiclin, Franjo Pernuš, Boštjan Likar, Tim Jerman, and Domen Ravnik. Dataset variability leverages white-matter lesion segmentation performance with convolutional neural network. In Elsa D. Angelini and Bennett A. Landman, editors, *Medical Imaging 2018: Image Processing*. SPIE, mar 2018.
- [46] M.D. Lawrence Steinman. Multiple sclerosis: A coordinated immunological attack against myelin in the central nervous system. *Cell*, 85(3):299–302, 2021/01/07 1996.
- [47] M. Strumia, F. R. Schmidt, C. Anastasopoulos, C. Granziera, G. Krueger, and T. Brox. White matter ms-lesion segmentation using a geometric brain model. *IEEE Transactions on Medical Imaging*, 35(7):1636–1646, 2016.
- [48] Vaanathi Sundaresan, Giovanna Zamboni, Peter M. Rothwell, Mark Jenkinson, and Ludovica Grifanti. Triplanar ensemble u-net model for white matter hyperintensities segmentation on MR images. 73:102184, October 2021.
- [49] A. Traboulsee, JH Simon, L Stone, E Fisher, DE Jones, A Malhotra, SD Newsome, Jiwon Oh, DS Reich, N Richert, et al. Revised recommendations of the consortium of ms centers task force for a standardized mri protocol and clinical guidelines for the diagnosis and follow-up of multiple sclerosis. *American Journal of Neuroradiology*, 37(3):394–401, 2016.
- [50] Sergi Valverde, Mariano Cabezas, Eloy Roura, Sandra González-Villà, Deborah Pareto, Joan C. Vilanova, Lluís Ramió-Torrentà, Àlex Rovira, Arnau Oliver, and Xavier Lladó. Improving automated multiple sclerosis lesion segmentation with a cascaded 3d convolutional neural network approach. *NeuroImage*, 155:159–168, jul 2017.
- [51] Sergi Valverde, Mostafa Salem, Mariano Cabezas, Deborah Pareto, Joan C. Vilanova, Lluís Ramió-Torrentà, Àlex Rovira, Joaquim Salvi, Arnau Oliver, and Xavier Lladó. One-shot domain adaptation in multiple sclerosis lesion segmentation using convolutional neural networks. *NeuroImage: Clinical*, 21:101638, 2019.
- [52] Yeeleng S Vang, Yingxin Cao, Peter D Chang, Daniel S Chow, Alexander U Brandt, Friedemann Paul, Michael Scheel, and Xiaohui Xie. Synergynet: a fusion framework for multiple sclerosis brain mri segmentation with local refinement. In *2020 IEEE 17th International Symposium on Biomedical Imaging (ISBI)*, pages 131–135. IEEE, 2020.
- [53] Olivier Vincent, Charley Gros, and Julien Cohen-Adad. Impact of individual rater style on deep learning uncertainty in medical imaging segmentation. *ArXiv*, abs/2105.02197, 2021.
- [54] Huisi Wu, Xiujuan Chen, Ping Li, and Zhenkun Wen. Automatic symmetry detection from brain mri based on a 2-channel convolutional neural network. *IEEE Transactions on Cybernetics*, 51(9):4464–4475, 2021.
- [55] Jie Xue, Kelei He, Dong Nie, Ehsan Adeli, Zhenshan Shi, Seong-Whan Lee, Yuanjie Zheng, Xiyu Liu, Dengwang Li, and Dinggang Shen. Cascaded multitask 3-d fully convolutional networks for pancreas segmentation. *IEEE Transactions on Cybernetics*, 51(4):2153–2165, 2021.
- [56] Yun Yang, Yuanyuan Hu, Xingyi Zhang, and Song Wang. Two-stage selective ensemble of cnn via deep tree training for medical image classification. *IEEE Transactions on Cybernetics*, 37(3):1–14, 2021.
- [57] Yun Yang, Yuanyuan Hu, Xingyi Zhang, and Song Wang. Two-stage selective ensemble of cnn via deep tree training for medical image classification. *IEEE Transactions on Cybernetics*, 2021.
- [58] Y. Yoo, T. Brosch, A. Traboulsee, D. Li, and R. Tam. Deep learning of image features from unlabeled data for multiple sclerosis lesion segmentation. In *MLMI*, 2014.
- [59] Hang Zhang, Jinwei Zhang, Rongguang Wang, Qihao Zhang, Susan A Gauthier, Pascal Spincemaille, Thanh D Nguyen, and Yi Wang. Geometric loss for deep multiple sclerosis lesion segmentation. In *2021 IEEE 18th International Symposium on Biomedical Imaging (ISBI)*, pages 24–28. IEEE, 2021.
- [60] Huahong Zhang and Ipek Oguz. Multiple sclerosis lesion segmentation - a survey of supervised cnn-based methods. In Alessandro Crimi and Spyridon Bakas, editors, *Brainlesion: Glioma, Multiple Sclerosis, Stroke and Traumatic Brain Injuries*, pages 11–29, Cham, 2021. Springer International Publishing.

- [61] Xiang Zhang, Xiaocong Chen, Lina Yao, Chang Ge, and Manqing Dong. Deep neural network hyperparameter optimization with orthogonal array tuning. In Tom Gedeon, Kok Wai Wong, and Minhoo Lee, editors, *Neural Information Processing*, pages 287–295, Cham, 2019. Springer International Publishing.
- [62] Mariana Zurita, Cristian Montalba, Tomás Labbé, Juan Pablo Cruz, Josué Dalboni da Rocha, Cristián Tejos, Ethel Ciampi, Claudia Cárcamo, Ranganatha Sitaram, and Sergio Uribe. Characterization of relapsing-remitting multiple sclerosis patients using support vector machine classifications of functional and diffusion MRI data. *NeuroImage: Clinical*, 20:724–730, 2018.
- [63] Özgün Çiçek, Ahmed Abdulkadir, Soeren S. Lienkamp, Thomas Brox, and Olaf Ronneberger. 3d u-net: Learning dense volumetric segmentation from sparse annotation. In *Medical Image Computing and Computer-Assisted Intervention – MICCAI 2016*, pages 424–432. Springer International Publishing, 2016.